ELSEVIER

International Journal of Mass Spectrometry 220 (2002) 253–262

International Journal of Mass Spectrometry

www.elsevier.com/locate/ijms

Photoelectron–photofragment coincidence spectroscopy of $NO_2^-(NO)_{1,2}$: solvation effects of NO on NO_2^-

A.K. Luong[1], T.G. Clements, R.E. Continetti*

Department of Chemistry and Biochemistry, University of California, San Diego, 9500 Gilman Drive, La Jolla, CA 92093-0340, USA

Received 7 November 2001; accepted 12 December 2001

Abstract

A study of the dissociative photodetachment dynamics of $N_2O_3^-$ and $N_3O_4^-$ at 258 nm is reported. Using photoelectron–photofragment coincidence (PPC) spectroscopy, information on the energetics and dissociation dynamics is recorded for both $N_xO_y^-$ species. The results indicate that these anions exist as $NO_2^-(NO)_{1,2}$ clusters, and dissociation occurs to form NO and NO_2 products upon photodetachment of the extra electron. It is shown that the energy released in the solvation of NO_2^- with one and two NO molecules is 0.23 ± 0.05 and 0.38 ± 0.05 eV, respectively. The photoelectron spectra show that solvation of NO_2^- by one NO does not significantly affect the electronic structure of the anion. The addition of a second NO to $NO_2^-(NO)$, however, leads to a suppression of photodetachment to the $\tilde{A}^2B_2$ excited state of NO_2 in the $NO_2(NO)_2$ cluster. The data also suggests that the three-body dissociation process of the larger cluster may occur via a sequential decay mechanism. (Int J Mass Spectrom 220 (2002) 253–262)

Keywords: Coincidence spectroscopy; Solvation; Nitrogen oxides; Photodetection

1. Introduction

Due to the abundance of nitrogen and oxygen in the Earth's atmosphere and the propensity for N–N, N–O, and O–O bonds to form, studies of nitrogen oxides have shown that these systems have a rich chemistry. The NO and NO_2 radicals predominantly exist as dimers in liquids and solid matrices and are best described as N_2O_2 and N_2O_4 [1,2]. Isomers of both species have been extensively studied experimentally and theoretically [3–6]. There have also been a number of studies of the cluster anions [7–12]. One of the important questions has been the nature of the bond that is formed between the two monomers. For example, Posey and Johnson [12] showed that the types of intramolecular bonds formed in N_2O_2 anions are source condition dependent. Other studies focused on the heterogeneous dimer clusters, such as $NO^-(N_2O)$ and $NO_2^-(NO)$ [13–17]. Pertinent to this work, early experiments on nitrogen oxides in the gas and matrix-isolated phases showed evidence for different isomers of N_2O_3, formed by dimerization of NO and NO_2 [1,3]. It has also been demonstrated that interconversion between the different isomers may occur upon photolysis. Varetti and Pimentel [2] showed that *asym*-N_2O_3 isomerizes to form *sym*-N_2O_3 with exposure to infrared radiation, which can convert back to the *asym*-form upon ultraviolet irradiation. Fig. 1

* Corresponding author. E-mail: rcontinetti@ucsd.edu

[1] Present address: Combustion Research Facility, Sandia National Laboratories, P.O. Box 969, Livermore, CA 94551-0969, USA.

1387-3806/02/$ – see front matter
PII S1387-3806(02)00773-X

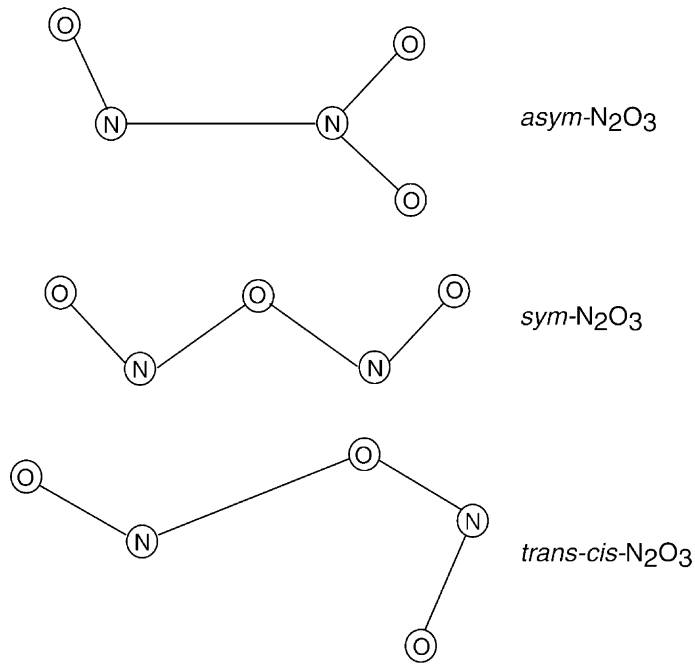

Fig. 1. Illustrations of some observed structural forms of N_2O_3.

illustrates the structures of the *asym*- and *sym*-forms of N_2O_3. However, these earlier studies were hindered by the presence of other nitrogen oxides.

Interest in the structural characteristics of these species led to infrared absorption experiments. Bibart and Ewing [18] studied the temperature dependence of the vibrational spectra of the stable form (*asym*) of gaseous N_2O_3. This study permitted the observation and assignment of all the vibrational frequencies of N_2O_3. More recently, Lee et al. [19] conducted Fourier-transform infrared absorption experiments of the N_2O_3 in solid argon, providing evidence for a *trans–cis* isomer after 308 nm irradiation of *asym*-N_2O_3. The *trans–cis* N_2O_3 was found to convert to *sym*-N_2O_3 following further irradiation with a Ne lamp ($\lambda > 630$ nm). The vibrational assignments for this new isomer were confirmed by density functional calculations (BLYP and B3LYP with basis sets from 6-31G* to cc-PVDZ). Using a semi-empirical valence bond calculation, Harcourt and Wolynec [20] suggested that the stability of the *asym*-N_2O_3, despite the experimentally determined long N–N bond length of 1.864 Å between the NO and NO_2 moieties, necessarily involves some charge transfer from the NO to the NO_2 radical.

There is far less work on N_2O_3 ions. Martin et al. [21] studied the formation of N_2O_3 cluster cations generated by laser ionization of a supersonic expansion of a $NO/CH_4/Ar/H_2O$ mixture. Their work suggests that the formation of the N_2O_3 cations involves a sequential mechanism, and depends on the presence of water and methane in the mixtures [21]. Recently, Chen et al. [22] reported theoretical calculations of the different isomers of $N_2O_3^-$. Using both B3LYP and MP2 methods, they determined that the anion structures also exhibit the *asym*, *sym*, and *trans–cis* structures. In addition, the results predicted the adiabatic electron affinity (AEA) of the *asym*, *sym*, and *trans–cis* isomers to be 2.43, 2.48, and 2.61 eV, respectively [22].

In the present study, we have carried out photoelectron–photofragment coincidence (PPC) studies of $NO_2^-(NO)_{1,2}$ clusters. The photoelectron and PPC spectra obtained show that the NO_2^- core persists

in these anion clusters. In $NO_2^-(NO)_2$, however, a significant shift in the electronic structure begins to be observed. The next sections give a brief account of the experimental apparatus, followed by the DPD results and discussion of the structure and dynamics of $N_2O_3^-$ and $N_3O_4^-$.

2. Experiment

In these experiments, PPC spectroscopy is applied to study the DPD dynamics of $N_2O_3^-$ and $N_3O_4^-$ anions. PPC spectroscopy combines photoelectron spectroscopy directly with photofragment translational spectroscopy, yielding complementary and kinematically complete information on two- and three-body DPD processes. Photodetachment of the anion precursor followed by detection of the photoelectron kinetic energy determines the energy of the transient neutral. Dissociation of the neutral complex produces fragments detectable by a multi-particle detector that measures the kinetic energies and recoil angles of all the photofragments produced in an individual event. This coincidence spectroscopy technique takes advantage of fast-ion beam methods and provides a kinematically complete probe of the DPD dynamics of the system of interest. The experimental technique has previously been described in detail in [23] and will be briefly described here.

The nitrogen oxide cluster anions were generated by crossing a supersonic expansion of a NO:Ne:He (0.17:0.20:0.63) gas mixture with a 1 keV electron beam. The anions passed through a skimmer, were accelerated to 4 keV, and mass selected by time-of-flight before entering the interaction region in an ultra high vacuum (UHV) chamber. Any neutrals generated before the UHV chamber were removed from the ion beam by use of a set of vertical deflectors and a neutral beam block. The linearly polarized third harmonic (258 nm) of a pulsed Ti:sapphire fundamental (1.2 ps FWHM) was focused to ∼0.5 mm, giving a fluence of 5–10 mJ/cm^2 per pulse, and crossed with the ion beam at 90°. Two opposed time- and position-sensitive photoelectron detectors aligned perpendicular to the ion and laser beam paths were used to detect the photoelectron with an angular acceptance of ∼20% of the full solid angle. The measured laboratory kinetic energies of the photoelectrons were corrected for the Doppler shift caused by the fast ion beam, yielding the center-of-mass (CM) electron kinetic energy (eKE). Calibration using the photoelectron spectrum of I^- at 258 nm indicated an eKE resolution of ΔeKE/eKE ∼ 5% at 0.8 eV.

The resulting neutral may undergo dissociation, generating photofragments that were detected in coincidence by a multi-particle time and position-sensitive detector located 104 cm downstream of the interaction region. Any ions remaining in the beam beyond the laser interaction region were electrostatically removed and detected by a MCP-based ion detector, which was also used to monitor the ion beam. The multi-particle detector for the neutral photofragments is comprised of four quadrants, each being a crossed-delay-line anode detector [24]. Each quadrant is capable of detecting the *x*, *y* positions and time-of-arrival of any two photofragments that are at least 10 ns apart. By conservation of linear momentum, the masses and CM kinetic energy and recoil angles of all the detected photofragments were determined for each event. The photofragment translational energy release, N(E_T), spectrum was obtained by a summation of the CM kinetic energy of the fragments, giving a resolution of $\Delta E_T/E_T$ ∼ 15% at 0.7 eV.

3. Results

3.1. Kinetic energy spectra

3.1.1. $N_2O_3^-$

As described in the previous section, the PPC technique permits the simultaneous measurement of the kinetic energies of the photodetached electron and any resultant neutrals from each individual photolysis event in the interaction region. This allows the construction of a photoelectron–photofragment energy correlation spectrum, N(E_T, eKE), yielding a two-dimensional histogram of the correlated events.

The observed distribution represents the partitioning of kinetic energy between the photoelectron and photofragments resulting from the DPD process. Integration over the *x*- or *y*-axis yields the N(eKE) and N(E_T) spectra, respectively. Finally, assuming that there is little internal energy in the parent anion (vibrationally and rotationally cold ground state anion), and that some products are generated with zero internal energy, a diagonal line drawn at the lowest contour indicates the maximum kinetic energy (KE_{MAX}) available to all the products. This KE_{MAX} value directly gives the DPD energy threshold of the anion. The location of this line, at 6% of the peak of the distribution, is determined by the rate of false coincidences for detecting a dissociation event under the experimental conditions [23].

Analysis of the $N_2O_3^-$ data showed that the only DPD channel accessed is the two-body dissociation leading to the formation of the products $NO + NO_2(\tilde{X}^2A_1, \tilde{A}^2B_2) + e^-$. Fig. 2 illustrates the N(E_T, eKE) for all the events with an E_T greater than 0.05 eV and an eKE greater than the laser-generated electron background (=0.20 eV), constituting approximately 40% of the recorded events. The electron background peak near 0 eV arises from scattered 258 nm photons on surfaces inside the machine. The N(E_T) distribution was observed to peak at ≈0 eV, which means that the presence of some stable neutral $NO_2(NO)$ clusters cannot be ruled out. The spectrum shown here is truncated below $E_T = 0.05$ eV to enhance the contrast of the contours. There are three diagonal lines drawn in the N(E_T, eKE) spectrum, indicating the KE_{MAX} values for the formation of $NO + NO_2(\tilde{X}^2A_1, \tilde{A}^2B_2 + \tilde{C}^2A_2) + e^-$ at 2.3, 1.12, and 0.46 eV, respectively. The contours show that there is no significant correlation between the photoelectron and photofragment translational energies, except for the conservation of energy. The distribution peaking at $E_T \approx 0$ eV shows that there is little repulsion between NO_2 and NO on the neutral surface, indicating that the structures of the anionic and neutral clusters are similar.

The N(eKE) spectrum of $NO_2^-(NO)$ is similar to that observed in photodetachment studies of NO_2^-. Fig. 3 shows the N(eKE) spectra for NO_2^-, $NO_2^-(NO)$ and $NO_2^-(NO)_2$ at 258 nm. The structures in the N(eKE) spectrum of NO_2^- have been previously assigned to photodetachment to the $\tilde{X}^2A_1$, $\tilde{A}^2B_2$, and $\tilde{C}^2A_2$ electronic states of the neutral

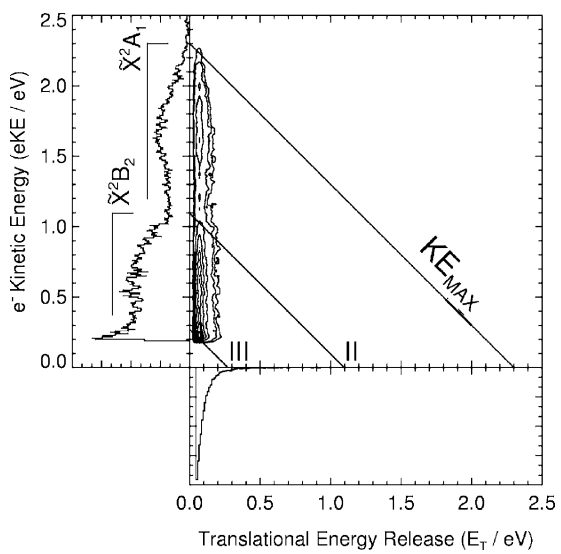

Fig. 2. The N(E_T, eKE) spectrum of $NO_2^-(NO)$ at 258 nm. The diagonal line labeled with KE_{MAX} indicates the maximum amount of kinetic energy available to form the products $2NO + NO_2$ in their ground states.

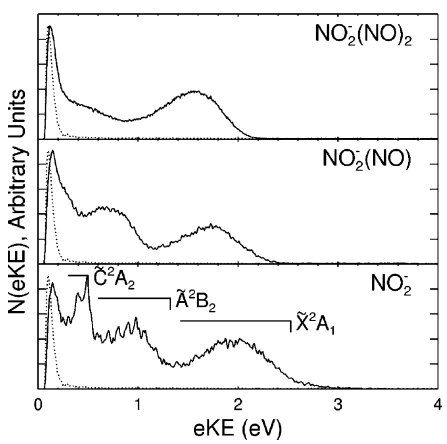

Fig. 3. The N(eKE) spectra of NO_2^-, $NO_2^-(NO)$ and $NO_2^-(NO)_2$ at 258 nm from the bottom to top frames, respectively. The dotted curve in each frame represents the laser-generated laser electron background noise and was recorded in a separate experiment.

[25,26]. The N(eKE) spectrum of NO_2^-(NO) exhibits features analogous to those of NO_2^- but without vibrational resolution. There is a shift of 0.23 eV to lower eKE at the peak of the feature corresponding to the production of $\tilde{X}^2A_1$ NO_2 in the complex. The resemblance of the N(eKE) spectrum of NO_2^-(NO) to NO_2^- strongly suggests that the excess electron is localized on the NO_2 moiety. Thus, $N_2O_3^-$ is best described as a weakly interacting NO_2^-(NO) ion–dipole complex rather than a covalently bound anion. The loss of vibrational structure in the $\tilde{A}^2B_2$ band for the NO_2^-(NO) photoelectron may be due to spectral congestion from low frequency modes in the complex. Note that the $\tilde{B}^2B_1$ electronic state is not observed, because the photodetachment from the ground anion to the $\tilde{B}^2B_1$ excited neutral state is not a one-electron transition [26,27]. The $\tilde{C}^2A_2$ state is energetically accessible, but is lost in the low energy photoelectron background produced by the laser.

Consideration of the available energy lends further support to the existence of a weakly interacting ion–dipole complex. Given the photon energy ($E_{h\nu}$) of 4.80 eV at 258 nm, the stability of the anion relative to the products can be determined by subtracting the maximum total kinetic energy ($E_{TOT} = E_T + eKE$), KE_{MAX}, of the products from $E_{h\nu}$. Because the anion is generated by clustering in a supersonic expansion, it is reasonable to assume that the internal energy of the parent anion is small. With an additional assumption that the resulting photofragments have little internal excitation, the relative stability of the anion is given by $E_{h\nu} - KE_{MAX}$. The N(E_{TOT}) spectrum is obtained by a summation of the eKE (above 0.20 eV to remove contributions from the electron background noise) and E_T for each individual event. The N(E_{TOT}) spectra for $N_2O_3^-$ is shown in the top frame of Fig. 4. The rising edge of the N(E_{TOT}) distribution curve at 2.30 eV is equal to KE_{MAX} shown in Fig. 2. This quantity shows that the anion is stable relative to the NO + NO_2 + e^- products by 2.50 ± 0.05 eV. Accounting for the AEA of NO_2 of 2.27 eV [25], the energy released in solvating NO_2^- with a single NO radical is thus 0.23 ± 0.05 eV.

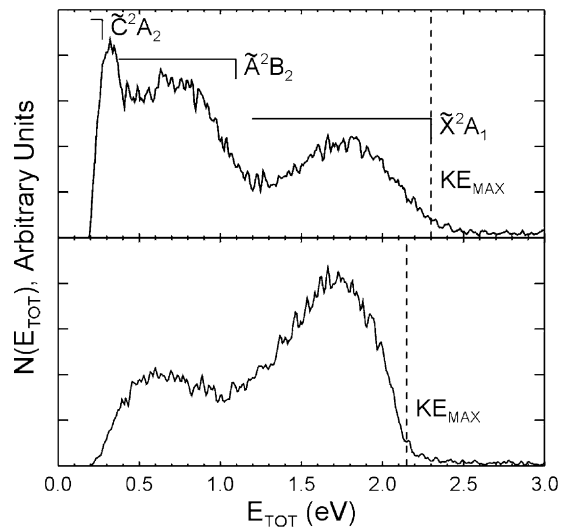

Fig. 4. N(E_{TOT}) spectra for NO_2^-(NO) and NO_2^-(NO)$_2$ at 258 nm in the top and bottom frames, respectively. The arrows indicate the KE_{MAX} values obtained from the N(E_T, eKE) spectra.

3.1.2. $N_3O_4^-$

The photoelectron–photofragment energy correlation spectrum for $N_3O_4^-$ at 258 nm is displayed in Fig. 5. Again, the spectrum is truncated below 0.20 eV

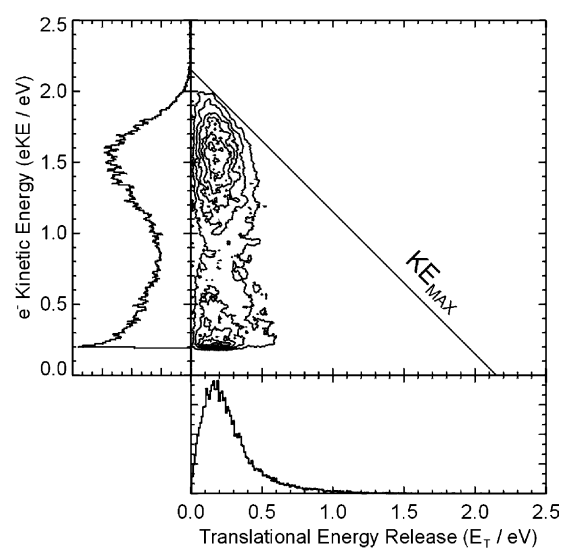

Fig. 5. The N(E_T, eKE) spectrum of NO_2^-(NO)$_2$ at 258 nm. The diagonal lines labeled with KE_{MAX}, II, and III indicate the maximum amount of kinetic energy available to forming the products 2NO + NO_2($\tilde{X}^2A_1$, $\tilde{A}^2B_2$, $\tilde{C}^2A_2$) + e^-, respectively.

along the *y*-axis to remove contributions from the electron background noise. Along the *x*-axis, Fig. 5 shows that the N(E_T) distribution peaks at a higher value of $E_T \approx 0.20$ eV in this case. The coincident N(eKE) spectrum along the *y*-axis only exhibits a broad peak at 1.6 eV, and a feature superimposed on the electron background noise signal below 1 eV. Except for a shift of ~0.1 eV lower in eKE, the shape and breadth of the peak at 1.6 eV is similar to that observed in the N(eKE) spectrum of $N_2O_3^-$. However, the $\tilde{A}^2B_2$ electronic state observed in the $N_2O_3^-$ N(eKE) spectrum is suppressed. The diagonal limit at $KE_{MAX} = 2.15$ eV shown in Fig. 5 indicates that the products are 2.65 ± 0.05 eV above the anion precursor. The energetics show that the three-body DPD process only produces the NO + NO + $NO_2(\tilde{X}^2A_1, \tilde{A}^2B_2)$ + e^- products. Accounting for the AEA(NO_2) of 2.27 eV, the NO_2^- + NO + NO product asymptote thus lies 0.38 ± 0.05 eV above $N_3O_4^-$. Thus, an additional 0.15 ± 0.05 eV is released when another NO solute molecule is added to the NO_2^-(NO) cluster.

Additional insights into the $NO_2^-(NO)_2$ cluster may be gained by comparison of the N(E_{TOT}) spectra between the two cluster anions. The comparison is shown in Fig. 4, with the normalized N(E_{TOT}) spectrum for $N_2O_3^-$ and the $N_3O_4^-$ in the top and bottom frames, respectively. This figure also shows that production of the $\tilde{A}^2B_2$ electronic state of the NO_2 moiety in the $NO_2(NO)_2$ neutral complex is suppressed in comparison to the electronic ground state. In addition, the rising slope of the peak assigned to photodetachment of the anion to the $\tilde{X}^2A_1$ ground state of NO_2 in the cluster is significantly steeper for the $N_3O_4^-$ than the $N_2O_3^-$. Although this characteristic is observable in the N(eKE) spectra in Fig. 3, it is more easily observed in the N(E_{TOT}) spectra in Fig. 4.

3.2. Molecular frame differential cross-section: $N_3O_4^-$

To aid in visualizing the three-body dissociation dynamics of $N_3O_4^-$, the molecular frame differential cross-section (MF-DCS) in momentum space may be constructed. Since the recoil vectors for the three-body dissociation necessarily form a plane in the CM frame, the MF-DCS is generated by transforming the laboratory frame momentum vectors for each fragment into the CM momentum vectors. The lightest and fastest fragment is selected as the reference particle and is aligned along the positive *x*-axis, while the vectors for NO_2 and the second, slower NO are distributed above and below the *x*-axis, respectively. If the dissociation is synchronous and originates from a single isomer, the distributions of the recoil vectors for the fragments show small relative angular spread, and can give direct insights into the structure of the complex, as in our previous DPD studies of $O_3^-(D_2O)$ at 258 nm [28]. However, this simple analysis of the MF-DCS spectrum may be hindered by the presence of multiple isomers or a long lived dissociation process. In both cases, it is expected that the correlation of the momentum vectors may be broadly distributed in the plane of the three-body dissociation.

Fig. 6 shows the MF-DCS spectrum of $NO_2(NO)_2$, which indicates that one NO recoils with the most momentum. The contour features for the slow NO and NO_2 fragments are diffuse with the centroid of each

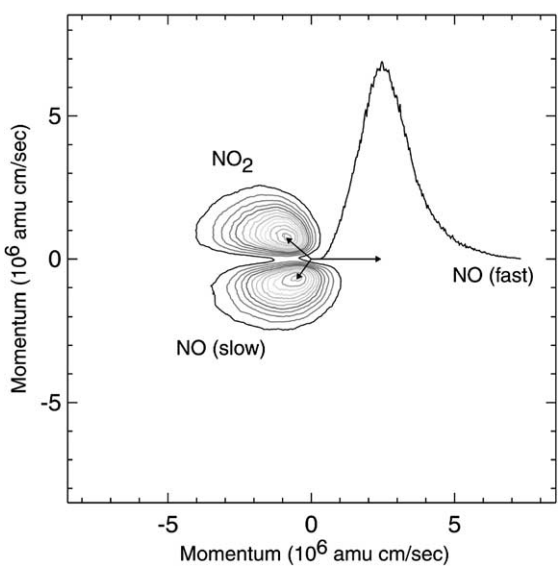

Fig. 6. The MF-DCS of $NO_2^-(NO)_2$ at 258 nm, where the arrows are drawn from the dissociation CM to the centroids of the momentum distributions of the three photofragments.

distribution at low momenta, and a gradual decrease in intensity towards higher momenta. Note that although conservation of linear momentum for each individual event (corresponding to three correlated momentum vectors in the MF-DCS spectrum) is achieved, the arrows drawn to the centroids of the one- and two-dimensional distributions in this figure do not appear to meet this constraint. This is a limitation of the MF-DCS in that the sum over all events shown in the spectrum does not apparently show conservation of momentum, even though the individual momentum vectors for each event do.

4. Discussion

The results for $N_2O_3^-$ and $N_3O_4^-$ at 258 nm demonstrate that, for each complex, the only isomer observed in our experiments is the weakly interacting ion–dipole cluster $NO_2^-(NO)_{1,2}$. In both complexes, the results are consistent with localization of the excess electron on the NO_2 moiety rather than the NO. These observations are in contrast to the experimental results for the heterogeneous cluster $N_3O_2^-$ reported by Sowa-Resat et al. [16] and Coe et al. [14]. In particular, Sowa-Resat et al. [16] found evidence of a covalently bound anion in addition to the ion–dipole complex. Furthermore, Coe et al. [14] showed that although the electron affinity of N_2O is higher than NO, and the HOMO of NO is an anti-bonding orbital, the extra electron resides near the NO moiety in the $N_3O_2^-$ complex. This has been suggested to be due to the large energy barrier (∼1 eV) to forming the N_2O anion. The energy barrier arises from the significant difference in the N–N–O bond angle between the N_2O anion and neutral. While the N_2O neutral is a linear molecule, the anion has an N–N–O bond angle of ∼134°. This factor does not come into play in the $NO_2^-(NO)$ cluster. However, the excess electron in NO_2^- does lead to a substantial decrease in the O–N–O bond angle and increase in the N–O bond length relative to neutral NO_2. The effects are apparent in the N(eKE) spectrum features of NO_2^-, which Weaver et al. [26] assigned to a progression arising from the bending and symmetric stretch modes of NO_2. The remarkable similarity between the N(eKE) spectra of $NO_2^-(NO)$ and NO_2^- clearly demonstrates that the geometry of NO_2^- is not significantly perturbed by the addition of a single NO.

The lack of strong correlation observed in the N(E_T, eKE) spectra and the low energy peak observed in the N(E_T) spectra also provides interesting insights into both cluster anions. In particular, the low E_T release indicates that dissociation of the neutral accessed by photodetachment is largely vibrationally and electronically adiabatic. There is very little conversion of the substantial electronic and vibrational energy deposited in the NO_2 moiety to translational degrees of freedom in the dissociation [29,30]. There is however another possible explanation for the appearance of the N(E_T, eKE) spectra of $NO_2^-(NO)$. The N_2O_3 neutral has been shown to be a stable, relatively strongly bound *asym* species in the gas phase with a dissociation energy (D_0) to form the NO and NO_2 monomers determined to be 0.41 eV experimentally and 0.36 eV theoretically [13,20]. This suggests that the observed N(eKE) spectrum may also arise from photodetachment to a weakly bound neutral species, which vibrationally predissociates to form $NO + NO_2 + e^-$. This dissociation mechanism is consistent with the observed E_T peak near 0 eV, and as noted before the production of some stable N_2O_3 complexes cannot be definitively ruled out. In any case, the low E_T observed shows that the region of neutral potential energy surface accessed is not very repulsive along the reaction coordinate. By subtracting the experimental $D_0(NO_2–NO)$ [13] from KE_{MAX} yields a value of 2.10 eV for the AEA of $NO_2(NO)$. The AEA estimated in this way is in reasonable agreement with the theoretical prediction of 2.43 eV for the *asym* structure as reported by Chen et al. [22]. The energy diagram in Fig. 7 summarizes the observed energetics for the two clusters.

The B3LYP and MP2 calculations by Chen et al. [22] estimated $D_0(NO–NO_2^-)$ to be 0.21 and 0.46 eV, respectively. Given this low dissociation energy, it is also possible that ionic photodissociation producing $NO + NO_2^-$ could occur at 258 nm. Unfortu-

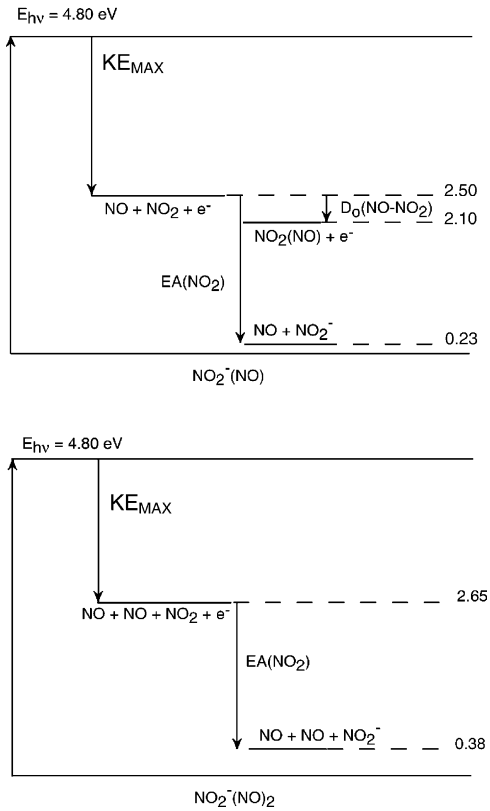

Fig. 7. Energy diagrams for $NO_2^-(NO)$ and $NO_2^-(NO)_2$ in the top and bottom frames, respectively. The experimental value for $D_0(NO–NO_2)$ was previously reported by Brittain et al. [13].

nately, the current apparatus can only detect this ionic photodissociation channel if the nascent NO_2^- absorbs a second photon and photodetaches. If this occurs, it is expected that the N(eKE) spectrum for $NO_2^-(NO)$ in Fig. 2 would exhibit signatures identical to NO_2^-. The absence of these features indicate that photodissociation of the cluster anion followed by absorption of a second photon in the 1.2 ps laser pulse to detach the excess electron does not occur.

The N(E_T, eKE) spectrum for $N_3O_4^-$ in Fig. 5 suggests that the addition of a second NO to $NO_2^-(NO)$ leads to an increased stability of 0.15 eV relative to the $NO_2^-(NO)$ cluster yet produces a more significant change in the electronic structure of the complex. These effects are observed in the distribution of neutral electronic states produced by photodetachment and the markedly higher E_T observed in the dissociation. There is evidently significantly larger repulsion in the nascent neutral $NO_2(NO)_2$ cluster, as the N(E_T) distribution peaks approximately 10 times higher than in $NO_2^-(NO)$. In addition, the relative intensities of the $\tilde{X}^2A_1$ and $\tilde{A}^2B_2$ peaks are inverted in the spectrum for $NO_2(NO)_2^-$ compared to both NO_2^- and $NO_2^-(NO)$. Production of the $\tilde{A}^2B_2$ state occurs when an electron is photodetached from the doubly filled $3b_2$ orbital in NO_2^-. It is possible that addition of the second NO to $NO_2^-(NO)$ affects the electron density in this orbital significantly, reducing the intensity of this electronic transition. An alternative view is to consider the effect of solvation on the doubly filled $4a_1$ highest-occupied molecular orbital (HOMO) of NO_2^-. The addition of NO molecules may lead to an increased localization of the diffuse anionic HOMO, increasing the relative propensity for photodetachment from the HOMO, producing the $\tilde{X}^2A_1$ ground state in the complex.

In addition to the effect on the electronic transition moment, the steeper slope of the $\tilde{X}^2A_1$ feature in the N(E_{TOT}) spectrum of $NO_2^-(NO)_2$ as compared to $NO_2^-(NO)$ in Fig. 4 suggests that the Franck–Condon vibrational distribution in the bend and symmetric stretch modes in the NO_2 moiety are significantly affected by the addition of the second NO. The $NO_2^-(NO)_2$ N(E_{TOT}) and N(eKE) spectra are consistent with less vibrational excitation produced in photodetachment of $NO_2^-(NO)_2$ to $\tilde{X}^2A_1$ $NO_2 + NO + NO$. It is interesting to note that the geometry for ground state NO_2^- ($r_{N–O} = 1.25$ Å, $\theta = 117.5°$) is closer to the $\tilde{A}^2B_2$ state (1.26 Å, 102°) than the $\tilde{X}^2A_1$ state (1.19 Å, 133.9°) of NO_2 [25–27]. Thus, it is expected that removal of electron density from the NO_2^- $4a_1$ HOMO will lead to an NO_2^- core in a geometry closer to the $\tilde{X}^2A_1$ state of NO_2, yielding a more vertical transition to this state. A quantitative explanation of these effects, however, awaits electronic structure calculations beyond the scope of the present work.

The MF-DCS provides another view of the dissociation dynamics of the $NO_2(NO)_2$ neutral cluster following photodetachment. The wide relative angular

distributions of the contour features coupled with the apparent lack of conservation of linear momentum in the correlated sum point to a decay mechanism either involving a distribution of initial geometries, leading to a wide distribution of relative scattering angles, or a sequential dissociation process in which the primary dissociation of the $NO_2(NO)_2$ complex produces an NO and an $NO_2(NO)$ transient intermediate which subsequently dissociates. This phenomenon was also previously observed in the MF-DCS spectrum of the three-body DPD of $O_2^-(H_2O)_2$ [30]. In those experiments, it was postulated that the breadth of the contours may arise from a sequential dissociation process, the presence of multiple conformers, or a combination of both.

5. Conclusion

Studies of the DPD of $NO_2^-(NO)_{1,2}$ clusters at 258 nm have quantified the solvation effects of NO addition to the NO_2^- anion. The energy released in solvating NO_2^- with one NO is 0.23 ± 0.05 eV, while the addition of two NO molecules releases 0.38 ± 0.05 eV. It was found that the N(eKE) spectrum of $NO_2^-(NO)$ is strikingly similar to that for NO_2^-, however, the spectrum for $NO_2^-(NO)_2$ reveals that photodetachment of the larger cluster produces the neutral with a significantly different distribution of electronic and vibrational energy. In particular, access to the low lying excited state, $\tilde{A}^2B_2$, is significantly suppressed while access to the $\tilde{X}^2A_1$ ground state is enhanced for $NO_2^-(NO)_2$. It is postulated that the additional NO stabilizes the anti-bonding HOMO of NO_2^- such that the electronic transition moment and Franck–Condon distribution is shifted to favor the $\tilde{X}^2A_1$ ground state while reducing production of the $\tilde{A}^2B_2$ state. Finally, the MF-DCS spectrum suggests that dissociation of the nascent $NO_2(NO)_2$ is not a synchronous process from a well-defined anionic geometry, and is likely broadened by a distribution of isomeric geometries and sequential dissociation processes. Further theoretical studies of the electronic structure and dissociation dynamics of these species are needed.

Acknowledgements

This work was supported by the Air Force Office of Scientific Research (AFOSR) under grant F49620-000-10-010. REC is a Camille Dreyfus Teacher-Scholar. Acquisition of the laser used in these studies was assisted by AFOSR DURIP grant F49620-97-1-0255.

References

[1] W.C. Fateley, H.A. Bent, J. Crawford, Bryce, J. Chem. Phys. 31 (1959) 204.
[2] E.L. Varetti, G.C. Pimentel, J. Chem. Phys. 55 (1971) 3813.
[3] I.C. Hisatsune, J.P. Devlin, Y. Wada, J. Chem. Phys. 33 (1960) 714.
[4] L. Burnelle, P. Beaudouin, L.J. Schaad, J. Phys. Chem. 71 (1967) 2240.
[5] F. Bolduan, H.J. Jodl, Chem. Phys. Lett. 85 (1982) 283.
[6] M. Kawasaki, K. Kasatani, H. Sato, H. Shinohara, N. Nishi, Chem. Phys. 78 (1983) 65.
[7] N.G. Adams, D.K. Bohme, D.B. Dunkin, F.C. Fehsenfeld, E.E. Ferguson, J. Chem. Phys. 52 (1970) 3133.
[8] J.F. Paulson, J. Chem. Phys. 52 (1970) 959.
[9] C.E. Klots, R.N. Compton, J. Chem. Phys. 69 (1978) 1636.
[10] H. Shimamori, R.W. Fessenden, J. Chem. Phys. 74 (1981) 453.
[11] M. Knapp, O. Echt, D. Kreisle, E. Recknagel, J. Chem. Phys. 85 (1986) 636.
[12] L.A. Posey, M.A. Johnson, J. Chem. Phys. 88 (1988) 5383.
[13] A.H. Brittain, A.P. Cox, R.L. Kuczkowski, Trans. Faraday Soc. 65 (1969) 1963.
[14] J.V. Coe, J.T. Snodgrass, C.B. Freidhoff, K.M. McHugh, K.H. Bowen, J. Chem. Phys. 87 (1987) 4302.
[15] K. Hiraoka, S. Fujimaki, K. Aruga, S. Yamabe, J. Phys. Chem. 98 (1994) 8295.
[16] M. Sowa-Resat, V. Zengin, M.C. Garner, R.E. Continetti, J. Phys. Chem. A 102 (1998) 1719.
[17] A. Snis, I. Panas, Chem. Phys. Lett. 305 (1999) 285.
[18] C.H. Bibart, G.E. Ewing, J. Chem. Phys. 61 (1974) 1293.
[19] C.-I. Lee, Y.-P. Lee, X. Wang, Q.-Z. Qin, J. Chem. Phys. 109 (1998) 10446.
[20] R.D. Harcourt, P.P. Wolynec, J. Phys. Chem. A 104 (2000) 2138.
[21] M.Z. Martin, S.R. Desai, C.S. Feigerle, J.C. Miller, J. Phys. Chem. 100 (1996) 8170.
[22] M. Chen, M. Zhou, Q. Qin, Chem. Phys. Lett. 321 (2000) 498.
[23] K.A. Hanold, A.K. Luong, T.G. Clements, R.E. Continetti, Rev. Sci. Instrum. 70 (1999) 2268.
[24] P.G. Friedman, R.A. Cuza, J.R. Fleischman, C. Martin, D. Schiminovich, D.J. Doyle, Rev. Sci. Instrum. 67 (1996) 596.

[25] K.M. Ervin, J. Ho, W.C. Lineberger, J. Phys. Chem. 92 (1988) 5405.
[26] A. Weaver, R.B. Metz, S.E. Bradforth, D.M. Neumark, J. Chem. Phys. 90 (1989) 2070.
[27] G.D. Gillispie, A.U. Khan, J. Chem. Phys. 63 (1975) 3425.
[28] A.K. Luong, T.G. Clements, R.E. Continetti, J. Phys. Chem. A 103 (1999) 10237.
[29] K.A. Hanold, R.E. Continetti, Chem. Phys. 239 (1998) 493.
[30] A.K. Luong, T.G. Clements, M. Sowa-Resat, R.E. Continetti, J. Chem. Phys. 114 (2001) 3449.